Acoustic Emission Source Localization in Fiber-Reinforced Composites based on Multimodal Dispersion Compensation of Guided Waves

ARNAUD HUIJER, CHRISTOS KASSAPOGLOU
and LOTFOLLAH PAHLAVAN

ABSTRACT

Fiber-reinforced composite materials are widely used in the aviation, civil, and shipbuilding industries. Especially the latter two industries are typically dealing with thicker composites. At the same time, in these industries the need for structural health monitoring, to assess degradation and failure, is becoming more prevalent. Acoustic emission (AE) measurement and analysis for damage source localization and characterization can be a useful method for the assessment of structural integrity for these structures.

In the case of composite panels, acoustic emissions can propagate in the form of elastic guided waves. The location of the AE source exposes regions in a structure that are subject to degradation. Typical acoustic emission source localization methods assume that the recorded AE signals consist of a single dominant fundamental wave mode. However, with thicker composites, the acoustic emissions may propagate in a multitude of modes. This will complicate the signal processing operations for accurate source localization.

This research assesses experimentally how guided wave multimodality influences acoustic emission localization. An acoustic emission source is excited in a thick glass fiber-reinforced plastic (GFRP) panel. Measurements from this excitation are first assessed for their content of higher modes. Source localization is carried out based on dispersion compensation through time-distance domain migration. Different possibilities and combinations of wave modes are considered. The localization error is assessed for each option. The results highlight the added complexity of multimodality and show how the inclusion of multiple modes into the procedure can improve the accuracy of source localization.

Arnaud Huijer, Faculty of Mechanical, Maritime and Materials Engineering, Delft University of Technology, Mekelweg 2, 2628 CD Delft, the Netherlands.
Christos Kassapoglou, Faculty of Aerospace Engineering, Delft University of Technology, Kluyverweg 1, 2629 HS Delft, Delft, the Netherlands.
Lotfollah Pahlavan, Faculty of Mechanical, Maritime and Materials Engineering, Delft University of Technology, Mekelweg 2, 2628 CD Delft, the Netherlands.

INTRODUCTION

Currently, there is widespread use of fiber-reinforced composite materials. This is especially the case in the aviation, civil, and shipbuilding industries. These materials can enable structures to be lighter, stronger, and more durable. In civil and shipbuilding industries, mostly thicker composites are in use. At the same time, these structures experience harsh conditions while inspection options are limited. Continuous structural health monitoring can therefore provide improved insight into the extent of degradation in these structures.

A promising method for structural health monitoring is by measuring acoustic emissions [1], [2]. An acoustic emission (AE) is an ultrasound elastic burst emanating from material degradation. Localization of the AE can be fundamental in the assessment of the structural health and the estimation of the remaining lifetime of the structure. Various methods for AE localization exist for fiber-reinforced composite materials [3]. One of these methods is time-distance domain migration (TDDM). This method maps the full waveform to a distance domain and then back-propagates this to account for dispersion [4]. On fiber-reinforced composites, Caj et al. [5], [6] used TDDM for processing active guided wave testing. Wilcox [7], Jiao et al. [8], de Marchi et al. [9] and Grabowski et al. [10] suggested a method to apply TDDM or similar for AE localization. These works performed back-propagation assuming the dispersion of a single dominant wave mode. In thicker composites, the AE can propagate in a multitude of wave modes, each having different dispersion characteristics and an unknown magnitude. This complicates AE localization as contributions of other wave modes will give an erroneous back-propagation. Xu et al. [11] and Wu & Wang [12] described multimodal back-propagation in thicker panels. They noted that back-propagation using a specific mode will compress and amplify the contribution of that mode in the measurement, streamlining further assessment.

This paper experimentally investigates AE localization using TDDM when multiple wave modes are present in the measurement. To do so, artificial AE with varying frequency content was excited in a 10.2mm thick glass-fiber reinforced plastic panel. This excitation was measured by a sensor that was at a known distance from the source. Dispersion characteristics of multiple wave modes have been used in the assessment. Localizations using individual wave modes and combinations of wave modes have been compared.

Firstly, the methodology is explained. This includes the evaluation of the measurements for their diversity of wave modes. Further, TDDM and multimodal processing are explained, along with the experimental procedure. Secondly, the results are described and interpreted. Thirdly, conclusions are drawn and recommendations are given.

METHODOLOGY

The degradation of material is often accompanied by the generation of AE. These are typically measured at a location away from the location of material degradation. Hence, the measured AE is subject to wave propagation effects. In the case of plate-like structures, the AE propagates in the form of guided waves. In the frequency domain, the relation between AE source and measurement can be cast into Equation 1 [13]:

$$P(\mathbf{x}_R, \mathbf{x}_S, \omega) = \sum_{i=1}^{n} D_i(\mathbf{x}_R, \omega) W_i(\mathbf{x}_R, \mathbf{x}_S, \omega) \varsigma_i(\mathbf{x}_S) S(\mathbf{x}_S, \omega) + P_N(\mathbf{x}_R, \omega) \quad (1)$$

Here, the source location is denoted by $\mathbf{x}_S$, the measurement location by $\mathbf{x}_R$ and the angular frequency by ω. The AE source signal $\varsigma_i(\mathbf{x}_S)S(\mathbf{x}_S,\omega)$ is convolved with wave propagation $W_i(\mathbf{x}_R,\mathbf{x}_S,\omega)$ and sensor electromechanical transfer $D_i(\mathbf{x}_R,\omega)$. Remark that the source and transfer functions are generally dependent on the wave mode i. In thick panels a multitude of modes may be supported. Measurement noise is denoted by $P_N(\mathbf{x}_R,\omega)$. The outcome is measurement signal $P(\mathbf{x}_R,\mathbf{x}_S,\omega)$. In the current context, the noise level is considered negligible and the sensor transfer function is assumed constant over frequency and wave mode. Wave propagation transfer $W_i(\mathbf{x}_R,\mathbf{x}_S,\omega)$ in an anisotropic medium can be described as in Equation 2:

$$W_i(\mathbf{x}_R, \mathbf{x}_S, \omega) = \alpha_i(\mathbf{x}_R, \mathbf{x}_S, \omega) e^{jk_i(\mathbf{x}_R, \mathbf{x}_S, \omega)x} \quad (2)$$

In this equation, $\alpha_i(\mathbf{x}_R, \mathbf{x}_S, \omega)$ is a scaling factor that includes attenuation effects due to radiation, damping and skewing. Change in signal phase and arrival time is covered by the exponential term. Here, angular wavenumber $k_i(\mathbf{x}_R, \mathbf{x}_S, \omega)$ is defined for the direction of $\hat{x} = (\mathbf{x}_R - \mathbf{x}_S) / \|\mathbf{x}_R - \mathbf{x}_S\|$.

Multimodal Acoustic Emission Localization

This research employs $W_i(\mathbf{x}_R,\mathbf{x}_S,\omega)$ to investigate the extent of multimodality in a measurement and to localize the source of the AE by accounting for this multimodality. The modal contribution, or extent of multimodality $\alpha_i(\mathbf{x}_R, \mathbf{x}_S, \omega)\varsigma_i(\mathbf{x}_S, \omega)$ can be assessed through comparison of $P(\mathbf{x}_R,\mathbf{x}_S,\omega)$ with $P^*(\mathbf{x}_R,\mathbf{x}_S,\omega)$ in Equation 3.

$$P^*(\mathbf{x}_R, \mathbf{x}_S, \omega) = \sum_{i=1}^{n} \alpha_i(\mathbf{x}_R, \mathbf{x}_S, \omega) \varsigma_i(\mathbf{x}_S) S(\mathbf{x}_S, \omega) e^{jk_i(\mathbf{x}_R, \mathbf{x}_S, \omega)x} \quad (3)$$

Here the source excitation $S(\mathbf{x}_S, \omega)$, measurement $P(\mathbf{x}_R,\mathbf{x}_S,\omega)$, dispersion relationship $k_i(\mathbf{x}_R, \mathbf{x}_S, \omega)$ and distance x are considered known. Single-mode localization is performed using TDDM as was described by Wilcox [4]. This involves back-propagation as per Equation 4:

$$R_i(\mathbf{x}_R, \mathbf{x}_S, \omega) = P(\mathbf{x}_R, \mathbf{x}_S, \omega) e^{-jk_i(\mathbf{x}_R, \mathbf{x}_S, \omega)x} \quad (4)$$

In order to evaluate Equation 4 in distance domain using the inverse Fourier transform, the right-hand side needs to be mapped from frequency domain to wavenumber domain. That is done using the group velocity $c_{gi}(\mathbf{x}_R, \mathbf{x}_S, \omega)$ as in Equation 5:

$$\begin{aligned} h_i(x) = &\int_{-\infty}^{\infty} R_i(\mathbf{x}_R, \mathbf{x}_S, \omega(k_i(\mathbf{x}_R, \mathbf{x}_S))) d\omega(k_i(\mathbf{x}_R, \mathbf{x}_S)) = \\ &\int_{-\infty}^{\infty} R_i(\mathbf{x}_R, \mathbf{x}_S, \omega(k_i(\mathbf{x}_R, \mathbf{x}_S))) c_{gi}(\mathbf{x}_R, \mathbf{x}_S, \omega(k_i(\mathbf{x}_R, \mathbf{x}_S))) dk_i(\mathbf{x}_R, \mathbf{x}_S) \end{aligned} \quad (5)$$

Here, distance domain reconstruction $h_i(x)$ is a measure of the distance travelled by a signal from the starting time of the measurement to the time of registration of the signal. The back-propagation compensates for dispersion. This implies that the wave mode that is present in the signal appears in the distance domain as relatively

compressed and with relative higher amplitude than in the time domain [11], [12]. This is the feature that is used for localisation. It is remarked that for such localisation the starting or onset time of the measurement should relate to the peak time of the source signal. In the case of measuring AE, this peak time of the source signal is unknown. Grabowski et al. [10] solved this by iteratively searching for the starting time that gave the most compressed back-propagation. In the current work, the starting time is not investigated and is considered known.

It is considered that a measurement signal contains contributions of a multitude of modes. The reconstruction using wave mode i will compress and amplify the contribution of that wave mode at the source location. However, the contributions of the other wave modes $j \neq i$ are also affected by the back-propagation. This means that artificial peaks can exist at locations that are different than the source location.

The multimodal localisation approach presented in this paper proposes to improve localisation by summation of reconstructions from a multitude of wave modes. Hilbert transform envelopes are used to largely exclude phase differences between the reconstructions. The summation can mitigate the severity of artificial peaks. This is because the contribution of mode i using reconstruction $h_i(x)$ will be at the same location for $i = 1..n$ whereas the artificial peaks are unlikely to be at the same location for $i = 1..n$. The approach is schematically visualised in Figure 1.

In the choice of wave modes to consider for localization, three options exist: The wave mode is present in the measurement, but not used for localization (A); The wave mode is present in the measurement, and used for localization (B); The wave mode is not present in the measurement, but is used for localization (C). The three options can be summarized in the Venn-diagram of Figure 1. All options are assessed.

Experimental Procedure

In order to investigate the feasibility of this multimodal localization approach, experiments have been performed on a thick glass-fiber reinforced polymer (GFRP) panel. The panel was instrumented with an actuator that generated a simulated AE signal, and a sensor that recorded the propagated AE. The actuator and sensor were both of the type VS600-Z1. They were coupled to the panel using ultrasonic gel and held in place using spline weights. The actuation signal was generated by an arbitrary waveform generator (Siglent SDG10251). This signal was directed to a power amplifier (Falco WMA-300, 34dB amplification) and to the data acquisition system (Vallen AMSY-6). The latter enabled direct assessment of the source signal peak time. From the power amplifier, the signal was conducted to the actuator. The sensor signal was amplified (Vallen AEPH5H, 40dB amplification) and recorded by the data acquisition system. A photograph of the set-up is shown with annotations in Figure 1.

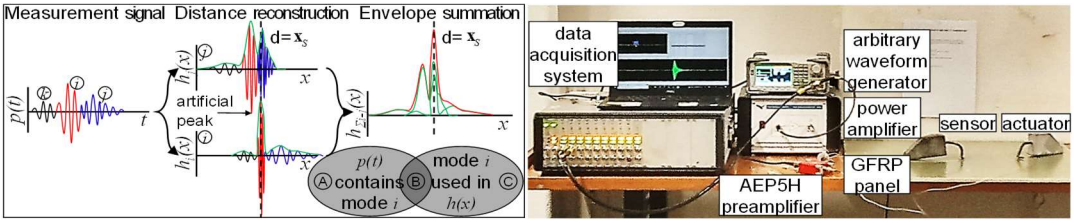

Figure 1. Schematic representation of localization using multimodal TDDM.

Property	Value
Modulus E_1, E_2= E_3 [GPa]	35.7, 10
Modulus G_{21} [Gpa]	2.8
Poisson's ratio ν_{21}, ν_{12}, ν_{32} [-]	0.325, 0.091, 0.35
Density ρ [kg/m^3]	1800

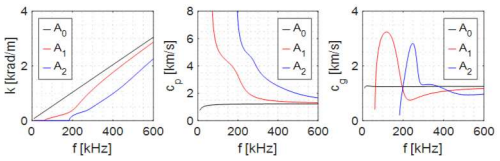

Figure 2. Material properties [14] and selected antisymmetric dispersion curves.

The GFRP panel had a 600mm length and width, was 10.2mm thick and had a [0 90]$_s$ lay-up.It was made of 640g/m^2 U-E glass from Saertex with an Atlac E-nova MA 6215 vinyl ester resin. Ambient-temperature vacuum-assisted resin transfer moulding was used. The panel was considered to have material properties similar to those used by Samaitis and Mažeika [14], and are shown in Figure 2. From these properties, dispersion curves have been calculated using a semi-analytical finite element method. In the localization procedure only antisymmetric modes (A_0, A_1, A_2) are used. This is because the actuator is placed on the surface of the panel. This promotes antisymmetric motion. The dispersion curves can be seen in Figure 2 for the 0˚ direction.

The data acquisition system recorded the signals in a hit-based manner, saving full waveforms with a 20MHz sampling frequency. A static threshold of 45dB was applied, based on the ambient noise level. This was complemented with a digital filter ranging from 20kHz to 960kHz. Rearm time and duration discretization time were set at 400µs and the pretrigger time at 500µs.

For actuation, a Hann-windowed sine function was used. Two signals were tested: one with 200kHz center frequency and four cycles, and one with 300kHz center frequency and six cycles. The actuator was placed in the center of the panel and the sensor was placed at distances of 75mm and 150mm away from the actuator in the 0˚ direction.

RESULTS AND DISCUSSION

The experimental data is analyzed in the following manner: Firstly, each measurement signal of the receiver sensor is assessed for their content in wave modes. This gives improved insight when discussing the localization results. Secondly, the signals are reconstructed in the distance domain representation for each wave mode separately. The distance value at the peak of the envelope of these reconstructions are estimates of the source location when considering a single mode. Thirdly, the envelopes are combined for a multimodal localization. Different combinations are assessed. Fourthly, localization errors are provided and assessed.

The contribution of the different wave modes present in the receiver sensor measurement signal is investigated. To do so, the emitted source $s(\mathbf{x}_S,t)$ was extrapolated forward in time using Equation 1. The results are propagated signals for the individual wave modes towards the location of measurement. The dispersion curves for the first three antisymmetric modes (Figure 2) were used. For a 300kHz center frequency signal at a distance of 150mm, the results are visualized in the first two graphs in Figure 3.
After the extrapolated signals $p_i^*(\mathbf{x}_R,\mathbf{x}_S,t)$ for the individual wave modes have been obtained, it was now possible to relate these to the signal that was actually measured ($p(\mathbf{x}_R,\mathbf{x}_S,t)$).This was done through assigning a contribution factor $\alpha_i\varsigma_i$ to each extrapolation and then summing the extrapolations ($\sum_i \alpha_i\varsigma_i p_i^*(\mathbf{x}_R,\mathbf{x}_S,t)$). Values for $\alpha_i\varsigma_i$

were approximated through visual similarity. The results are pictured in the right graphs of Figure 3. Table I provides the values for each source-receiver distance and center frequency. In the table, it may be seen that for the 200kHz center frequency cases, there appears to be no contribution of mode A_2. This enables assessment of localization in the case of situation 3 defined in the Venn diagram in Figure 1 (i.e. a mode is used in the reconstruction that is not present in the original signal). In the other measurements, it is apparent that there is a more balanced contribution to each mode. Note that in the current measurement frequency range, mode A_0 is relatively non-dispersive and has the largest contribution in terms of amplitude. This is especially the case with the 200kHz center frequency measurements.

The signals measured by the receiver sensor were reconstructed through TDDM as per Equation 5. The starting time of the excitation was considered known and was calculated directly from the excitation signal. In Figure 4, the distance domain results per individual mode $h_i(\mathbf{x}_R,\mathbf{x}_S,x)$ are shown together with their respective envelopes. The fourth graph visualizes the summation of the three reconstructions $\sum_i h_i(\mathbf{x}_R,\mathbf{x}_S,x)$ and the summation of the individual envelopes. From the figure, it may be seen that the envelopes of the individual reconstructions show several peaks. In the cases of wave mode A_0 and A_2, the largest peaks are around the source location (x=150mm) while in A_1, the largest peak is at a smaller distance. Smaller secondary peaks are present as well. The locations of these peaks can be explained through the dispersion curves in Figure 2. Mode A_0 around 300kHz is almost nondispersive. Hence the reconstruction is similar to the measurement signal. The largest amplitude of the signal is provided by A_0, and therefore the localization peak for A_0 is at the source location. For A_1, the group velocity is lower than that of A_0. Also it is not very dispersive. This implies that when reconstructing with A_1, the peak in the signal that corresponds to A_0 is localized at a shorter distance than the source location distance. Note also that this peak is higher and the reconstruction contains less lobes than when reconstructing with A_0. This implies that reconstruction of the A_0 component using A_1 dispersion creates artificial focusing. However, there is furthermore a secondary peak, relating to the A_1 contribution, that is correctly localizing around the source location. Wave mode A_2 has strong dispersive characteristics around 300kHz. In the reconstruction for A_2 this becomes visible as a strong 'tail' between 200mm and 400mm.

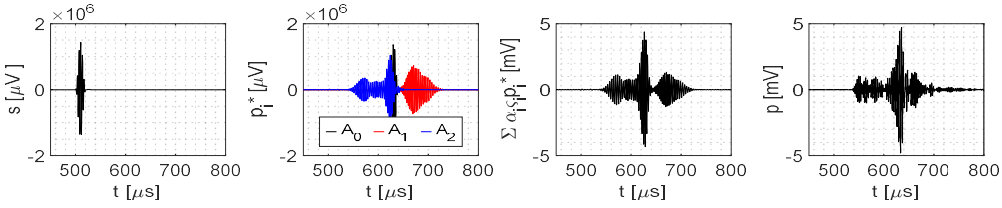

Figure 3. Measurement of a wave excitation and evaluation of multimodality.

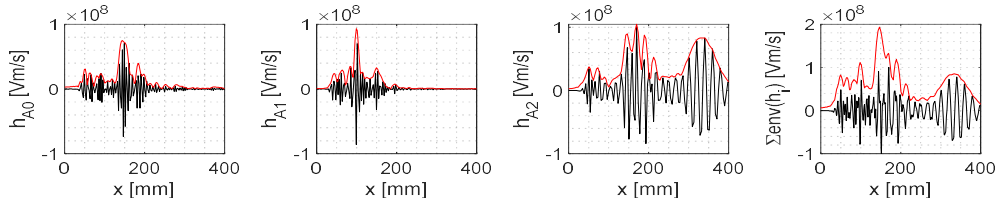

Figure 4. Distance domain reconstructions per individual mode and the summation.

TABLE I. TIME-DISTANCE DOMAIN LOCALISATION ERROR

$\|\|\alpha_i\varsigma_i\|\|$ [%]					εd_i [mm]					$\varepsilon d_{\Sigma i}$ [mm]				
x [mm]	75		150			75		150			75		150	
f_c [kHz]	200	300	200	300		200	300	200	300		200	300	200	300
$\|\|\alpha_0\varsigma_0\|\|$	55	48	59	23	εd_0	6	3	2	-6	$\varepsilon d_{\Sigma 01}$	-22	-3	-53	-1
$\|\|\alpha_1\varsigma_1\|\|$	45	30	41	28	εd_1	-24	-27	-51	-51	$\varepsilon d_{\Sigma 12}$	94*	-3^+	176*	-3^+
$\|\|\alpha_2\varsigma_2\|\|$	0	22	0	49	εd_2	91*	33	178*	20	$\varepsilon d_{\Sigma 012}$	25*	-4	173*	-3

This is likely coming from the contribution of A_0 that is now strongly (inversely) dispersed. Note that for A_2, the maximum peak is around the source location. This is indicative of correct reconstruction of the A_2 contribution. The combination of reconstructions, shown in the bottom right graph, appears to not give a satisfactory reconstruction of the source signal. This is mainly attributed to slight variations between the used dispersion curves and the actual material. This causes phases to be slightly misaligned. The combination of envelopes nevertheless is not adversely affected by this issue and the peak at the source location stands out.

Values of the envelope peak location have been assessed for a 200kHz and a 300kHz signal, measured at 75mm and 150mm. The errors between the estimated and true location are given in Table I. In Table I, εd_i denotes envelope peak location error using wave mode i. Similarly $\varepsilon d_{\Sigma ijk}$ describes peak location error for the combination of envelopes for wave modes i, j and k. Values with an asterisk (*) relate to the third region in the Venn diagram of Figure 1, while plusses (+) relate to the first region.

In all cases, reconstruction with A_0 gives a low error εd_0 amounting to 1.3% to 8% of the distance. This is considered reasonable, because the A_0 has the largest amplitude component and is nondispersive. Reconstruction with A_1 in all situation gives an erroneous result. This is due to the lower contribution of A_1 and that the dispersion curve for A_1 tends to artificially focus the A_0 contribution. For reconstruction with A_2, the 200kHz signal is not properly localized. This is because there is no A_2 component in the original signal (*). At 300kHz, the localization is improved, but still with low precision. This may partly be attributed to small variations between modelled and actual material properties.

For combined results $\varepsilon d_{\Sigma i\text{-}k}$ it is clear that the 200kHz reconstruction remains biased by the reconstructions of εd_1 and εd_2 (29% to 125% error). For the 300kHz signal peak locations are close to the source location (2% to 5.3% error). The availability of the A_2 mode, and different dispersion behaviour of A_1, are the cause of this. In this respect, the case of $\varepsilon d_{\Sigma 12}$ is particularly interesting. Here localisation was performed without taking into account the accurate A_0 reconstruction (+ values, first region of Figure 1). Notwithstanding, the peak location has a small error with the source location. This implies that multimodal reconstructions can be better in localisation than using a single mode reconstruction.

For future research it is recommended to add the determination of onset time, as per for example Grabowski [10], since this will likely be affected by the multimodality.

CONCLUSIONS

Distance domain reconstruction was studied for multimodal localization of acoustic emissions in a GFRP panel. It was found that in the situation of a known dominant wave mode, single mode reconstruction can give results with a reasonably small error (1.3%

to 8%). Multimodal localization can give results with a small error (2% to 5.3%) when there is a balanced contribution of multiple wave modes. However it is prone to a larger error (29% to 125%) when there are few wave modes contributing to the received signal and one wave mode is dominant. It is recommended that for forthcoming research the effect of multimodality on the quality of onset time picking of the AE is investigated.

ACKNOWLEDGEMENTS

The authors would like to acknowledge The Netherlands Organization for Scientific Research (NWO) (project number 18463) and project partners for both funding and technical input. Additionally Sajad Alimirzaei is acknowledged for his contribution to the development of the used semi-analytical finite element method.

REFERENCES

[1] Scheeren, B., Kaminski, M. L., and Pahlavan, L., (May 2023), "Acoustic emission monitoring of naturally developed damage in large-scale low-speed roller bearings," *Struct. Heal. Monit.*

[2] Alkhateeb, S., Riccioli, F., Morales, F. L., and Pahlavan, L., (Dec 2022), "Non-Contact Acoustic Emission Monitoring of Corrosion under Marine Growth," *Sensors*, vol. 23, no. 1, p. 161

[3] Hassan, F. *et al.*, (2021), "State-of-the-Art Review on the Acoustic Emission Source Localization Techniques," *IEEE Access*, vol. 9, pp. 101246–101266

[4] Wilcox, P. D., (2003), "A rapid signal processing technique to remove the effect of dispersion from guided wave signals," *IEEE Trans. Ultrason. Ferroelectr. Freq. Control*, vol. 50, no. 4, pp. 419–427

[5] Cai, J., Shi, L., and Qing, X. P., (2013), "Erratum: A time-distance domain transform method for Lamb wave dispersion compensation considering signal waveform correction (Smart Materials and Structures (2013) 22)," *Smart Mater. Struct.*, vol. 22, no. 11

[6] Cai, J., Wang, X., and Zhou, Z., (2019), "A signal domain transform method for spatial resolution improvement of Lamb wave signals with synthetically measured relative wavenumber curves," *Struct. Heal. Monit.*, vol. 18, no. 5–6, pp. 1633–1651

[7] Wilcox, P., "Application of guided wave signal processing to acoustic emission data," in *AIP Conference Proceedings*, Apr. 2005, vol. 760, pp. 1809–1816.

[8] Jiao, J., He, C., Wu, B., and Fei, R., (Jul 2004), "A new technique for modal acoustic emission pipeline leak location with one sensor," *Insight Non-Destructive Test. Cond. Monit.*, vol. 46, no. 7, pp. 392–395

[9] De Marchi, L., Marzani, A., Speciale, N., and Viola, E., (Mar 2011), "A passive monitoring technique based on dispersion compensation to locate impacts in plate-like structures," *Smart Mater. Struct.*, vol. 20, no. 3

[10] Grabowski, K. *et al.*, (2016), "Time-distance domain transformation for Acoustic Emission source localization in thin metallic plates," *Ultrasonics*, vol. 68, pp. 142–149

[11] Xu, K., Ta, D., Moilanen, P., and Wang, W., (Apr 2012), "Mode separation of Lamb waves based on dispersion compensation method," *J. Acoust. Soc. Am.*, vol. 131, no. 4, pp. 2714–2722

[12] Wu, W. and Wang, Y., (Apr 2019), "A Simplified Dispersion Compensation Algorithm for the Interpretation of Guided Wave Signals," *J. Press. Vessel Technol. Trans. ASME*, vol. 141, no. 2

[13] Pahlavan, L., Mota, M. M., and Blacquière, G., (Sep 2016), "Influence of asphalt on fatigue crack monitoring in steel bridge decks using guided waves," *Constr. Build. Mater.*, vol. 120, pp. 593–604

[14] Samaitis, V. and Mažeika, L., (2017), "Influence of the spatial dimensions of ultrasonic transducers on the frequency spectrum of guided waves," *Sensors (Switzerland)*, vol. 17, no. 8